Int. J. Electrochem. Sci., 9 **(2014)** 7832 - 7845

International Journal of
ELECTROCHEMICAL
SCIENCE
www.electrochemsci.org

Enhanced Corrosion Resistance of SS304 Stainless Steel and Titanium Coated with Alternate Layers of TiN and ZrN in a Simulated O_2-rich Environment of a Unitized Regenerative Fuel Cell

Meng-Tsun Lin[1], *Chieh-Hao Wan*[2,*] *and Weite Wu*[1,**]

[1] Department of Materials Science and Engineering, National Chung Hsing University, 250 Kuo Kuang road, Taichung 402, Taiwan, R.O.C.
[2] Department of Materials and Energy Engineering, MingDao University, 369 Wen-Hua road, Peetow, Changhua 52345, Taiwan, R.O.C.
[*]E-mail: chiehhao@mdu.edu.tw;
[**]E-mail: weite@dragon.nchu.edu.tw

Received: 16 September 2014 / *Accepted:* 13 October 2014 / *Published:* 28 October 2014

In this study, alternative layers of titanium nitride/zirconium nitride (TiN/ZrN) were coated on the surface of SS304 stainless steel and titanium (Ti) to enhance their corrosion resistance in a simulated oxygen (O_2)-rich environment of a unitized regenerative fuel cell (URFC). The cathodic arc evaporation physical vapor deposition (CAE-PVD) technique was used to coat the multilayers. The effect of the O_2 on the electrochemical behavior of the TiN/ZrN-coated SS304 and Ti in the O_2-rich environment with acid and fluoride (F^-) ions was investigated. The results showed that the TiN/ZrN coating with a nano-composite structure improved the corrosion resistance about 243 and six times, respectively, as compared with uncoated Ti and SS304 in the O_2-rich environment with F^- ions and acid. This coating also increases the corrosion potential of Ti from 0.097 to 0.302 V and that of SS304 from -0.085 to 0.080 V. These coatings outperformed CrN and TiN coatings on SS316L or Ti surfaces in an O_2-rich environment. The improved results are due to the dense columnar microstructure of the nano-composite TiN/ZrN layer, which provides strong chemical protection from the hydrogen (H^+) and F^- ions, even in the presence of O_2, thereby preventing any direct corrosive attack on the substrate. The presence of O_2 in the solution containing the F^- ions and acid slightly increased the corrosion rate of the TiN/ZrN layer as compared to that of hydrogen gas.

Keywords: Unitized regenerative fuel cell; cathodic arc evaporation; physical vapor deposition technique; nano-composite TiN/ZrN layer; metal bipolar plate

1. INTRODUCTION

The use of fuel cells in movable or portable devices and in transportation has become very attractive because of their high energy-conversion efficiency and environmental compatibility. Researchers have combined fuel cells and electrolyzers into one unit to produce a unitized regenerative fuel cell (URFC) with the aim of reducing the weight and volume of devices [1]. Electrolyzers offer a clean, easy, and effective way to produce hydrogen (H_2) gas using water as the anode and cathode fuel [2]. URFCs work first in the electrolyzer mode to store H_2 and then use the H_2 in the fuel cell mode. Thus, an URFC behaves like a battery, with a self-contained, independent power source. However, in contrast to battery systems, URFCs are unaffected by the depth of the discharge or the length of the cycle duration. Therefore, in the long term, many applications exist for URFCs, such as an independent power source in a house or in a space without electricity access. Key advances required for the development of URFCs are 1) the creation of a bifunctional O_2 electrode with high catalytic activity in both fuel cell and electrolyzer modes and 2) the creation of a bipolar plate with reduced weight, volume and high corrosion resistance for use in O_2 reduction and water oxidation modes [1, 3]. To overcome the first challenge, many studies have focused on the development of highly active electrocatalysts, such as $PtIrO_2$ and $PtRuO_2$ [4, 5], for both O_2 reduction and water oxidation at the O_2 electrode. To address the second challenge, researchers are developing metal bipolar plate with improved corrosion resistance by surface modification techniques to protect the metal surface from corrosion [6-7].

Graphitic material is a typical bipolar plate material that is widely used in proton exchange membrane fuel cells (PEMFCs). However, in the water electrolyzer mode operated at higher potential (> 2V), graphite bipolar plates show severe corrosion at the contact area between the carbon bipolar plate and the electrode [8, 9]. This increases the ohmic resistance and decreases the performance of URFCs [10]. Bipolar plates with a metal base have been used to replace nonporous graphite bipolar plates because of their mechanical strength, excellent manufacturability, nonpermeability, recyclability, high thermal and electric conductivity, and cost effectiveness [11]. These metallic materials include stainless steel [12, 13], copper alloy [14, 15], titanium (Ti) [16], aluminum (Al) [17], and nickel clad [18]. Among these materials, stainless steel has received much attention as a bipolar plate material because of its relatively good corrosion resistance and low price. However, the corrosion resistance of stainless steel is poor when this metal operates at high potential and current in an acid- and O_2-rich environment of a URFC. Various coatings, such as Cr-based multilayers [19], compact titanium carbide (TiC) [20], molybdenum nitride (MoN) [21], titanium nitride (TiN) [22], zirconium nitride (ZrN) [23, 24], and titanium nitride/zirconium nitride (TiN/ZrN) multilayers [23, 25-27], have been deposited on the surface of stainless steel to improve its corrosion resistance. The TiC and TiN coatings reduced the corrosion current density compared to uncoated stainless steel (245 [20] and 108 times [22], respectively).

Ti has good mechanical strength, it can resist acidic corrosion, and it does not corrode in more positive over-potential under humidified conditions. However, the surface of Ti reacts readily with O_2 to form a passive oxide layer in the cathode-side environment of a fuel cell, thereby increasing the contact resistance, resulting in poor cell performance [2, 16]. Coatings of gold [16, 28], platinum [2], a

Ti-silver alloy [29], and TiN [30] have been deposited on the surface of Ti to prevent the formation of an oxide layer and improve the corrosion resistance of the Ti metal.

The O_2 electrode side of a URFC has a low pH value and is rich in O_2 gas when URFC operated in the electrolyzer mode. Wang et al. [31] investigated the effect of O_2 and H_2 gases on the corrosion of an SS316L bipolar plate in a simulated anode and cathode environment of PEMFCs. They showed that less corrosion of SS316L occurred in the O_2-rich environment because a passive oxide layer was formed on the surface of the SS316L in this environment. They further studied the effects of O_2 and H_2 gases on the corrosion of TiN-coated SS316L. [32] They found that the corrosion current density increased from 8.0×10^{-6} A cm^{-2} to 2.5×10^{-5} A cm^{-2} because pitting corrosion took place on the TiN-coated sample. Omrani et al. [33] showed an improvement in the corrosion resistance of about 945 times when TiN nanoparticles were implanted on SS316L compared to that of untreated SS316L tested in an O_2-rich environment with acid (i.e., 1.0 M H_2SO_4 at 70° C in an O_2-rich environment). Wang et al. [21] also showed that the corrosion current density of MoN-coated SS304 dropped from 1.35×10^{-5} A cm^{-2} to 3.83×10^{-6} A cm^{-2} in an O_2-rich environment with acid, indicating an improvement of about 3.5 times.

F^- ions exist in the anode- and cathode-side of fuel cells due to deterioration of the perfluorinated ionomer electrolyte membrane during the operation of the cells. As reported by Kong et al. [34], aggressive inorganic ions, such as F^-, that exist in an acid environment can attack the passivity of Ti and its alloys. They studied the anodic dissolution kinetics of Ti at open circuit potentials in 1.0 M $HClO_4$ solutions containing different concentrations of F^-. They reported that the F^- ions attacked the passivity of Ti and its alloys when the concentration of ions was more than 1×10^{-3} M. Therefore, it is important to study the electrochemical behavior of metal bipolar plates in an acid environment containing F^- ions.

In summary, the effect of O_2 gas on the corrosion of coated stainless steel depends on what kinds of coatings are deposited on the metal. Although many studies have examined the effect of O_2 on the electrochemical behavior of stainless steel, few have investigated the impact of O_2 on coated Ti. Of the studies that have been conducted, most were concerned with the mechanical performance of coated Ti rather than the potentiodynamic polarization of coated Ti. Furthermore, there is a lack of research on nitride coatings containing both Ti and Zr elements, especially their electrochemical behavior in a simulated URFC environment in the presence of O_2 gas. Therefore, this paper investigated the effect of O_2 gas on the electrochemical behavior of a nitride coating with a Ti and Zr nano-composite structure. We deposited the nano-composite structure consisting of alternate TiN/ZrN layers on SS304 and Ti plates using the cathodic arc evaporation physical vapor deposition (CAE-PVD) technique. The electrochemical behaviors of the samples were studied in an O_2-rich environment in an acid solution containing F^- ions.

2. EXPERIMENTAL DETAILS

Figure 1 shows a diagram of the proposed coatings. Ti_2N was used as the bottom layer for the substrates (SS304 and Ti), and TiN was used as the middle layer. These were then coated with a nano-composite of TiN/ZrN. The thickness of the two layers (bottom Ti_2N and middle TiN layers) was about 300 nm, which is much smaller than that of the TiN/ZrN coatings (2.60 μm).

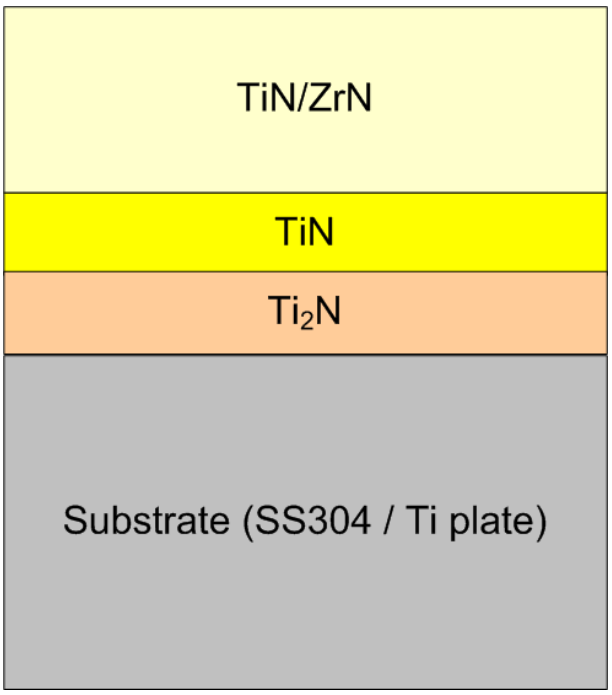

Figure 1. Diagram of the proposed layer structure that deposited on SS304 or Ti substrate.

2.1 Coating process of the TiN/ZrN layer

Commercialized SS304 stainless steel (composition: C: 0.08%, Mn: 2.0%, Si: 0.75%, Ni: 8–12%, Cr: 18–20%, N: 0.1%, S: 0.03%, P: 0.045%, Fe: balance) and Ti plates (composition: C: 0.008%, Mn: 0.012%, N:0.003%, Fe:0.02%, Al: 0.02%, Ti: balance) were used in this study. Before the coating processes, all the samples (20 mm × 30 mm × 1 mm) were polished with silicon carbide paper (No. 240# to 2400#) grit on a grinder and then with 0.30–0.05 μm Al_2O_3 powder on rubbing fur. The samples were coated after thorough degreasing, cleaning with detergent and deionized water, and drying in a hot oven.

Table 1. The parameters used in the deposition process.

Coating Parameters	**Setting value**
Ar ion bombardment	-800 V bias for 20 min
Substrate bias voltage / -V	120, 80
Substrate temperature / °C	150~200
Evaporator current / A	60
Chamber pressure / Pa	1~3
Reaction gas	N_2
Source to substrate distance / mm	150~180
Deposition time / minutes	
Ti_2N layer	1
TiN layer	5
TiN/ZrN layer	30

To prepare the TiN/ZrN multilayer, we used a dual-target CAE-PVD system, which is the same as that used in our earlier publication [35] . Similar coating processes and parameters to those used in [35] were applied in the current study. Briefly, the surface of the substrate was further cleaned with Argon ion bombardment under a bias voltage of -800 V for 20 minutes at a chamber pressure below 1.0 Pa. The bottom Ti_2N interlayer was deposited on the substrate according to the experimental parameters listed in Table 1 for 1 min. The second TiN interlayer was obtained by adjusting the chamber pressure and deposition time. Finally, the TiN/ZrN composite layer was deposited on top of the TiN interlayer using the parameters given in Table 1. The resulting samples were denoted as TiN/ZrN-coated SS304 for the SS304 stainless steel and TiN/ZrN-coated Ti for the Ti substrates. The TiN/ZrN coating was formed by alternate TiN and ZrN layers with almost the same layer thickness (i.e., 9.7 nm versus 10.2 nm) to produce a nano-composite structure. This TiN/ZrN coating (2.6-μm thick) with a dense columnar structure was strongly bonded with the substrate using the cathodic arc evaporation techniques. The detailed microstructure, morphology, and composition of the TiN/ZrN coating were reported in our earlier publication [35].

2.2 Characterization of the deposited layers

The potentiodynamic polarizations of the samples and substrates were measured in a homemade electrochemical corrosion test cell [35] by a potentiostat manufactured by EG&G (model: 263A). An exposed area of 1 cm^2 of the sample served as the working electrode, the Pt mesh served as the counter electrode, and an Ag/AgCl electrode served as the reference electrode in the test cell. The measurements were conducted in 250 ml of 0.50 M H_2SO_4 with 3 ppm of NaF, bubbled with O_2 gas at a flow rate of 10 standard cubic centimeter per minute (sccm, volume measured at 0 °C, 1 atm) under a scanning rate of 0.50 mV s^{-1} from -800 mV to 700 mV at 60° C. The polarization curves were recorded after the samples had stabilized at a corresponding open circuit potential for 60 min. It took about 6 h to complete the potentiodynamic polarization measurement. After the polarization testing, the corrosive solution was collected, and the amounts of Fe, Ni, Cr, Ti, Zr, and Mn ions dissolved in the solutions were analyzed with an inductively coupled plasma-mass spectrometer (ICP-MS) (Model: Agilent 7500ce, Agilent). The corroded samples were thoroughly washed with ultrapure water (18.2 MΩ cm) to remove any residues on the surface of the samples. After drying in an oven at 80° C for 24 h, the surface morphology of the samples was examined. A four-point probe apparatus was used to measure the surface resistance of the samples coated with TiN/ZrN and the uncoated samples at 25° C. The surface resistance of the samples was determined by passing a current through the two outer probes placed on the surface of the sample and measuring the voltage through the two inner probes. The sheet resistance is equal to the obtained surface resistance multiplied by 4.53 (the correction factor value) [37], and the resulting unit is in ohms per square (Ω sq^{-1}). A field-emission scanning electron microscope (FE-SEM) (model: JSM 7000F, JOEL) was used to analyze the microstructure of the deposited thin films before and after the potentiodynamic polarization measurements.

3. RESULTS AND DISCUSSION

3.1 Electrochemical polarization

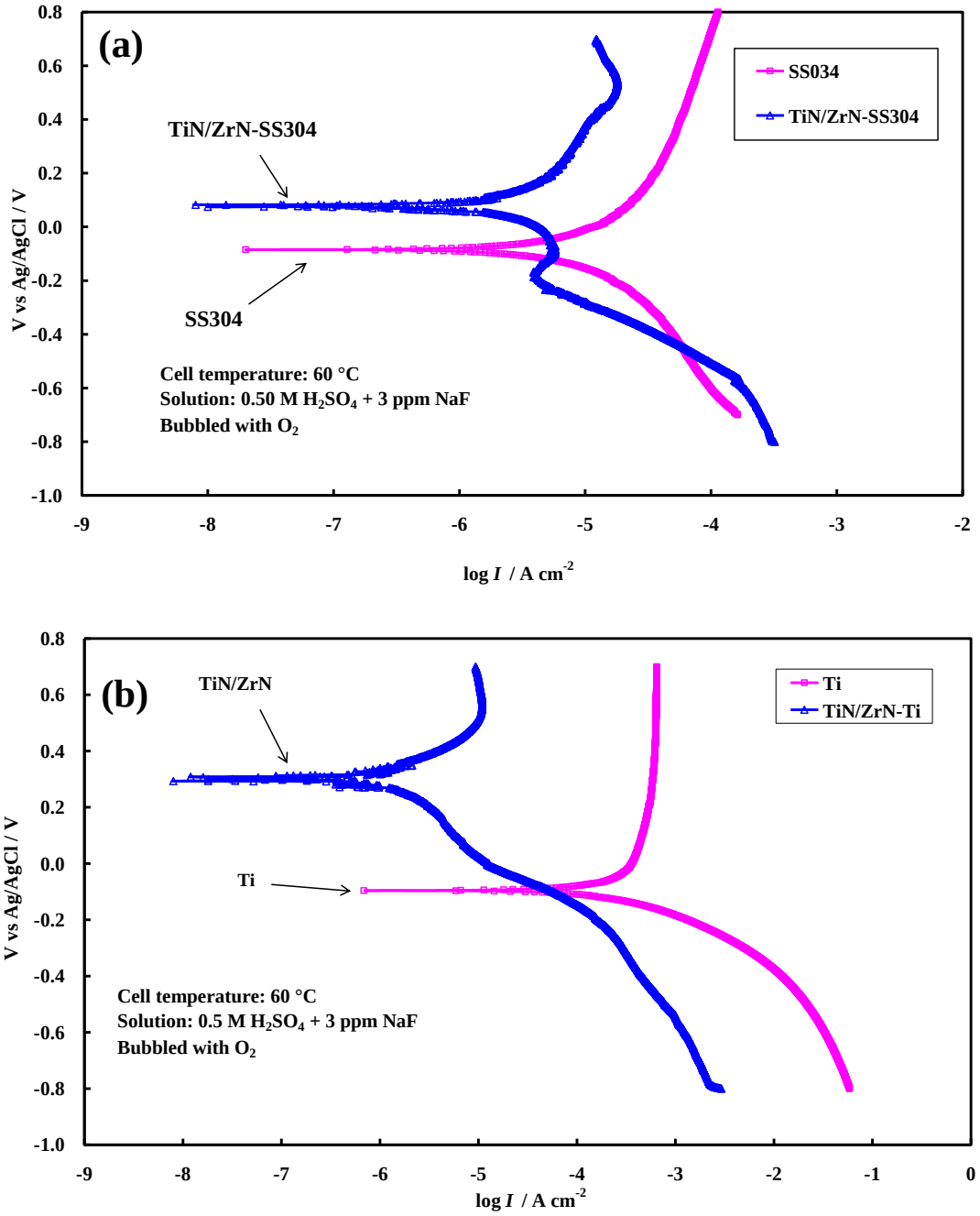

Figure 2. Potentiodynamic polarization curves of (a) TiN/ZrN-coated SS304 sample and SS304 substrate, and (b) TiN/ZrN-coated Ti sample and Ti substrate tested in 0.50 M H_2SO_4 with 3 ppm NaF solution bubbled with O_2 at 60 °C.

To investigate the corrosion current density (I_{corr}) of the studied samples, the I_{corr} was determined from the cross point of the anodic Tafel slope and the cathodic Tafel slope of the corresponding potentiodynamic polarization curves. In this study, the values of the β_a and the β_c were

obtained using the curve-fitting functions provided in EG&G software. The I_{corr} presented here is the average value over 10 runs of the curve-fitting results. The polarization resistance (R_p) of the samples was calculated using Equation 1 below:

$$Rp = \frac{\beta a \beta c}{2.3 I corr(\beta a + \beta c)} \quad (1)$$

where R_p is the polarization resistance calculated in Ω cm^2, β_a is the anodic Tafel slope calculated in mV, β_c is the cathodic Tafel slope calculated in mV, and I_{corr} is the corrosion current density calculated in A cm^{-2}.

Figure 2 and table 2 show the potentiodynamic polarization curves and corrosion electrochemical parameters of the bare SS304, Ti, TiN/ZrN-coated SS304, and TiN/ZrN-coated Ti. The I_{corr} of the TiN/ZrN-coated SS304 samples was about 49 times lower than that of the uncoated SS304 (i.e., 6.8×10^{-7} A cm^{-2} versus 3.3×10^{-5} A cm^{-2}). The I_{corr} of the sample with the TiN/ZrN coating and that of the bare Ti was 9.8×10^{-7} A cm^{-2} and 3.4×10^{-4} A cm^{-2}, respectively, indicating that the corrosion rate of the TiN/ZrN coating on Ti was about 345 times lower than that of the bare Ti. Due to the increased decrement in the I_{corr} of the TiN/ZrN coating on the Ti compared to that of the TiN/ZrN coating on the SS304 substrate, we conclude that the reduction in the corrosion rate of the TiN/ZrN coating on the Ti substrate is superior to that of the coating on the SS304 substrate. The R_p values further support this inference, with the TiN/ZrN-coated Ti showing an increment of 233 times versus an increment of six times for the TiN/ZrN-coated SS304 (as listed in Table 2).

Table 2. Polarization parameters of TiN/ZrN-coated SS304, TiN/ZrN-coated Ti, uncoated SS304 and Ti measured in 0.50 M H_2SO_4 with 3 ppm NaF solution and bubbled with O_2 at 60 °C.

Specimens	E_{corr} / V	I_{corr} /A cm^{-2}	β_a / mV	β_c / mV	R_p / Ω cm^2
SS304	-0.085	3.3×10^{-5}	1459	913	7.5×10^{3}
TiN/ZrN-coated SS304	0.080	6.8×10^{-7}	110	104	4.5×10^{4}
Ti	-0.097	3.4×10^{-4}	1579	149	1.8×10^{2}
TiN/ZrN-coated Ti	0.302	9.8×10^{-7}	154	201	4.3×10^{4}
SS304*	-0.424	3.7×10^{-6}	1127	789	5.2×10^{4}
Ti*	0.284	2.9×10^{-8}	814	813	6.1×10^{6}

* The samples tested in solution only containing the 0.50 M H_2SO_4 bubbled with O_2 at 60 °C.

Comparison of the I_{corr} between the bare SS304 and Ti revealed that the corrosion rate of the bare Ti was higher than that of the SS304. This implies that the corrosion resistance of SS304 is higher than that of bare Ti in an O_2-rich environment with F^- ions (i.e., 7.5×10^3 Ω cm^2 versus 1.8×10^2 Ω cm^2). This finding is contrary to that reported in some studies in the literature [37]. To clarify the source of the discord, we performed additional potentiodynamic measurements of the two samples using a solution containing only 0.50 M of H_2SO_4, bubbled with O_2 at 60° C (i.e., without F^- ions). The potentiodynamic curves and corrosion electrochemical parameters are shown in Figure 3 and Table 2, respectively. It can be seen that the I_{corr} of the bare Ti is about 127 times lower than that of the SS304

(i.e., 2.9×10^{-8} A cm^{-2} versus 3.7×10^{-6} A cm^{-2}), indicating that the corrosion rate of the bare Ti in the presence of O_2 and acid is lower than that of the SS304.

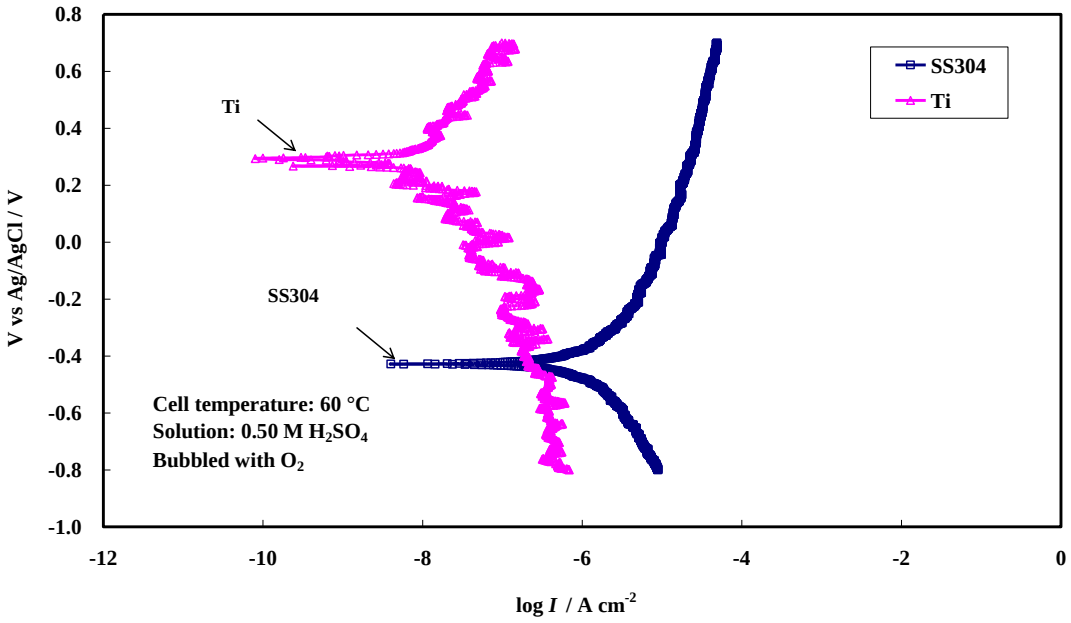

Figure 3. Potentiodynamic polarization curves of bare SS304 and Ti tested in 0.50 M H_2SO_4 solution and bubbled with O_2 at 60 °C.

This result is consistent with the reports in the literature [37]. The finding can be explained by the formation of a passive oxide layer on the surface of the Ti substrate in the presence of O_2, thereby preventing the acid corrosive medium from attacking the substrate directly. Obviously, the F^- ions strongly affected the corrosion rates of the bare Ti substrate. The corrosion rate of the Ti in the solution containing the F^- ions was much higher than that in the solution without the F^- ions (i.e., 3.4×10^{-4} A cm^{-2} versus 2.9×10^{-8} A cm^{-2}). On the other hand, we previously reported [35] that the I_{corr} of bare Ti in a H_2-rich solution with F^- ions was 3.5×10^{-6} A cm^{-2}. This I_{corr} value is 97 times lower than that recorded in the O_2-rich solution with the F^- ions in the present study, suggesting that the O_2 gas in the solution also affected the corrosion rate of Ti.

Summarizing the above results, the corrosion rate of Ti was enhanced in the solution containing the F^- ions and O_2 gas. The most probable explanation is that F^- ions destroyed the passive Ti oxide layer and reacted with the Ti substrate to form a Ti–F^- compound [34]. As a result, the corrosion rate of the bare Ti was higher than that of the bare SS304 in the acid solution containing the F^- ions and O_2.

3.2 Morphology

Figure 4 shows the SEM images of the corrosion of the TiN/ZrN-coated SS304 and uncoated SS304 after the potentiodynamic polarization testing in 0.50 M of H_2SO_4 with 3 ppm NaF, bubbled with O_2 gas. As shown in Figure 4(b), serious localized corrosion and corrosion by-products were

visible on the surface of the bare SS304. However, corrosion was only observed on the surface of TiN/ZrN coating at specific locations, as shown in Figure 4(d). This type of corrosion is known as pitting-type localized corrosion. Comparing Figures 4(c) and (d), we find that the corrosion of the TiN/ZiN layer mainly starts from defects such as micro-particles and pinholes, and these defects were scattered on the surface of the TiN/ZrN coating by the arc-sputtering process. We infer that galvanic corrosion takes place at those defect sites and that small anodic defect sites rapidly penetrate through the substrate. Accordingly, the numbers of microparticles and pinholes, as well as the penetration rate of small anodic defects, determine the corrosion resistance of the TiN/ZrN coating.

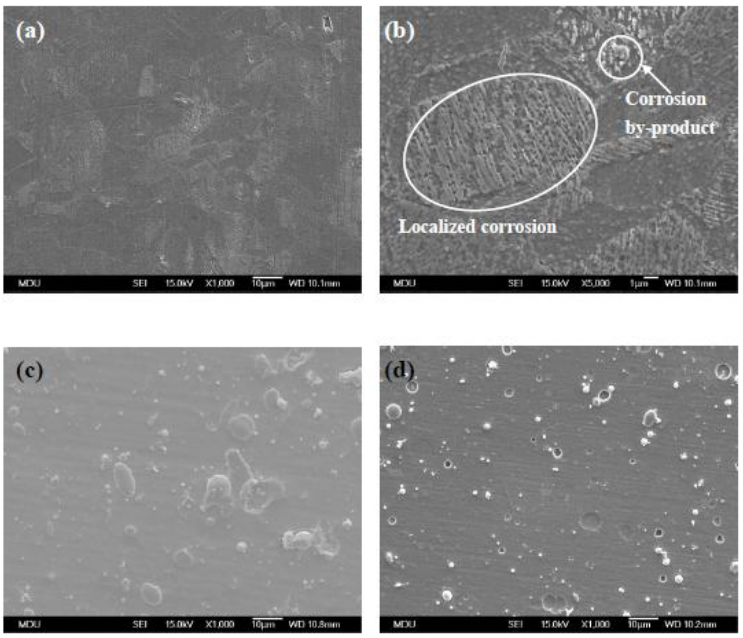

Figure 4. SEM images for the (a) bare SS304 (x1k), (b) bare SS304 (x5k) after the potentiodynamic polarization test, (c) TiN/ZrN-coated SS304 sample before and (d) after the potentiodynamic polarization test in the simulated URFC oxygen environment.

Table 3. The concentrations of dissolved ions in the corrosive solution after the polarization measurements for the TiN/ZrN-coated SS304, TiN/ZrN-coated Ti samples, uncoated SS304 and Ti.

	Dissolved ion concentration/ ppb					
Samples	Ti	Cr	Mn	Fe	Ni	Zr
TiN/ZrN-coated SS304	47.0	29.5	6.4	465.5	25.6	5.8
TiN/ZrN-coated Ti	75.5	----	----	----	----	19.7
SS304	----	309.8	205.9	11790.4	1322	----
Ti	100.6	22.4	5.2	----	----	----

Table 3 lists the dissolved ions found in the solution 6 h after the potentiodynamic polarization testing by ICP-MS analysis. The solutions of the TiN/ZrN-coated SS304 contained 47.0 ppb of Ti and 5.8 ppb of Zr ions. Small amounts of Fe (465.5 ppb), Cr (29.5 ppb), Mn (6.4 ppb), and Ni (25.6 ppb) ions were also present in the solutions of the TiN/ZrN-coated SS304 samples. These were derived from the SS304 substrate. This result evidently shows that the TiN/ZrN coating has a low degree of dissolution compared to that of the bare SS304.

Figure 5 depicts the SEM images of the corrosion morphology of the Ti substrate and TiN/ZrN-coated Ti. As shown in Figure 5(b), the Ti substrate showed more serious localized corrosion compared to the SS304 substrate. This observation supports the electrochemical polarization results, which demonstrated that the I_{corr} of the bare Ti was about 10 times higher than that of the SS304. However, as shown in Figure 5(d), the corrosion morphology of the TiN/ZrN-coated Ti is similar to that of the TiN/ZrN-coated SS304, suggesting that similar electrochemical behavior occurred on the surface of the TiN/ZrN coating. The results of the ICP-MS analysis showed a low degree of dissolution of the TiN/ZrN coating on the Ti (as shown in Table 3). Thus, the TiN/ZrN nano-composite layer appears to strongly impede anodic dissolution of SS304 or Ti, coupled with H^+ ion/O_2 reduction.

3.3. Sheet resistance (R_s)

Table 4. The sheet and surface resistances for TiN/ZrN-coated SS304, TiN/ZrN-coated Ti, uncoated SS304 and Ti samples.

Specimens	Surface resistance / mΩ	Sheet resistance (R_s) / mΩ sq^{-1}.
SS304	0.46	2.09
TiN/ZrN-coated SS304	0.65	2.95
Ti	0.45	2.04
TiN/ZrN-coated Ti	0.63	2.86

The surface resistance, which is the electric resistance of a thin film or surface, was determined with a four-point probe apparatus. Table 4 lists the surface and sheet resistances (R_s) of the uncoated substrates, TiN/ZrN-coated SS304, and TiN/ZrN-coated Ti. The surface and sheet resistances of SS304 slightly increased, from 0.46 mΩ to 0.65 mΩ and from 2.09 mΩ sq^{-1} to 2.95 mΩ sq^{-1} (mΩ sq^{-1} represents mili-ohms per square), respectively, following the application of the TiN/ZrN coating. The surface and sheet resistances of the TiN/ZrN layer coated on the Ti surface also slightly increased, from 0.45 mΩ to 0.63 mΩ and from 2.04 mΩ sq^{-1} to 2.86 mΩ sq^{-1}, respectively. These results indicate that the TiN/ZrN coating slightly decreased the electron conductivity of the SS304 and Ti substrates.

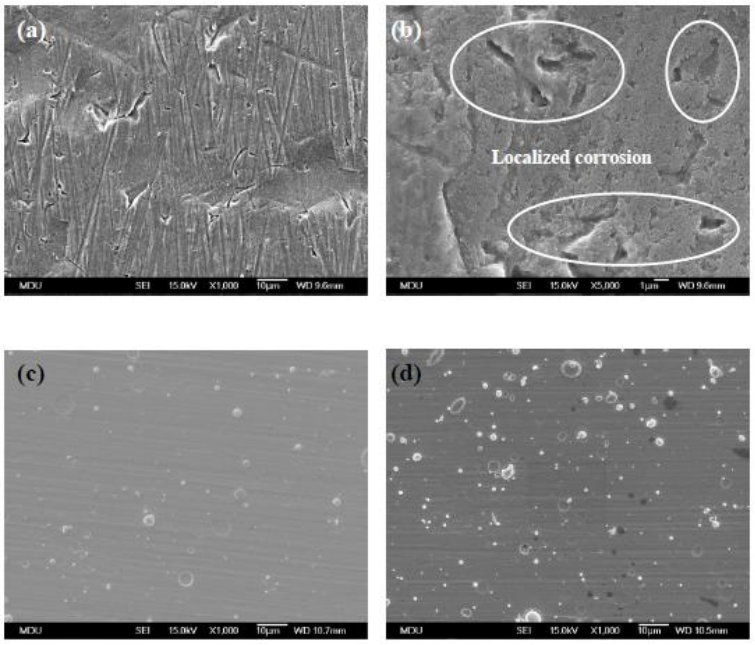

Figure 5. SEM images for the (a) bare Ti (x1k), (b) bare Ti (x5k) after the potentiodynamic polarization test, (c) TiN/ZrN-coated Ti sample before and (d) after the potentiodynamic polarization test in the simulated URFC oxygen environment.

The E_{corr} of SS304 in the O_2-rich environment was -0.085 V, which was about four times higher than that in the H_2-rich environment. The I_{corr} of SS304 was also lower in the O_2-rich environment than in the H_2-rich environment (i.e., 3.3×10^{-5} versus 4.0×10^{-5} A cm^{-2}). Thus, the rate of the anodic dissolution of SS304 in the O_2-rich environment was lower than that in the H_2-rich environment due to the presence of O_2, which forms a passive oxide layer protecting SS304. After coating the TiN/ZrN layer on the SS304, the corrosion current density decreased from 3.3×10^{-5} to 6.8×10^{-7} A cm^{-2}, indicating that the corrosion rate of the TiN/ZrN-coated SS304 decreased 49 times compared to the uncoated SS304. The difference in the corrosion rate is due to the dense columnar microstructure of the nano-composite TiN/ZrN layer, which is almost impermeable to corrosive media, such as H^+, SO_4^{2-}, and F^- ions. The nano-composite layer also provides strong protection against the H^+ and F^- ions, even in the presence of O_2. Therefore, it is difficult for the corrosive ions to penetrate the surface of SS304 and induce anodic dissolution of the metal. In contrast, the corrosion current density of the same coating on SS304 substrate in an H_2-rich environment [37] was reported to be lower than that in an O_2-rich environment (i.e., 3.1×10^{-7} A cm^{-2} versus 6.8×10^{-7} A cm^{-2}). The findings indicate that the presence of O_2 slightly enhances the corrosion rate of a TiN/ZrN coating in a corrosive solution containing F^- and H^+ ions.

Based on the electrochemical potentiodynamic results for Ti in the O_2-rich environment, with and without F^- ions, as well as the results of the SEM images after the potentiodynamic test, the corrosion current density of bare Ti was high in the O_2-rich environment due to the existence of F^- ions, although the concentration of the F^- ions was only 3 ppm. In contrast, the TiN/ZrN-coated Ti showed superior corrosion resistance to the corrosive medium in the O_2-rich environment containing F^- and H^+ ions. This is due to the dense columnar microstructure of the TiN/ZrN nano-composite layer providing

strong chemical protection against the F^- and H^+ ions, even in the presence of the O_2 gas. Of note, the corrosion current density of the TiN/ZrN-coated Ti in the O_2-rich environment was slightly higher than that in the H_2-rich environment (i.e., 9.8×10^{-7} A cm^{-2} versus 2.1×10^{-7} A cm^{-2}). This result implies that the presence of O_2 has a positive effect on the corrosion rate of the TiN/ZrN layer.

Comparing the increment in the R_p values of the TiN/ZrN-coated SS304 in O_2 environment in present study with those in H_2 environments in our earlier study [35], the increase was 215 times higher in the H_2 environment in the previous study. Nevertheless, the corrosion resistance of the TiN/ZrN-coated SS304 fulfills the requirement of a bipolar plate material for URFCs because its I_{corr} is lower than 10^{-6} A cm^{-2} (the target of the Department of Energy, USA). The increment in the R_p values of the TiN/ZrN-coated Ti in the O_2 environment was higher than those in the H_2 environment [35] (243 times versus 192 times, respectively). The great improvement in the corrosion resistance means that the TiN/ZrN-coated Ti substrate may be suitable as a bipolar plate material for URFCs.

Comparing the decrement in the I_{corr} of the TiN/ZrN-coated SS304 (from 3.3×10^{-5} to 6.8×10^{-7} A cm^{-2}) in this study with TiN-coated SS316L (from 4.3×10^{-5} to 1.0×10^{-6} A cm^{-2}) prepared by Wang [32], our coating outperforms the TiN coating, with the I_{corr} being 59 times lower in Wang's study. Thus, the performance of TiN/ZrN nano-composite layers is better than that of TiN layers in an O_2-rich environment. Comparison of the decrement in the I_{corr} of our TiN/ZrN-coated sample with that of a sample coated with a CrN layer developed by Pozio et al. [38] shows that the I_{corr} of the TiN/ZrN coating is lower (i.e., 49 times versus five times). Summarizing the above results, the corrosion resistance of the TiN/ZrN coating in this study outperforms the corrosion resistance of CrN and TiN coatings on an SS316L surface in an O_2-rich environment. The I_{corr} of the TiN-coated Ti substrate using the multi-arc ion plating [30] method was 8.6×10^{-9} A cm^{-2}, which is only five times lower than that of the uncoated Ti (4.2×10^{-8} A cm^{-2}). In contrast, the I_{corr} of our Ti sample with the TiN/ZrN coating decreased 345 times compared to the uncoated Ti substrate. Clearly, the TiN/ZrN coating outperforms the TiN coating on a Ti substrate in an O_2-rich environment containing F^- ions.

4. CONCLUSIONS

The corrosion resistance of the samples coated with alternate multilayers of TiN/ZrN on SS304 and Ti increased six and 243 times, respectively, compared to the uncoated SS304 and Ti in an O_2-rich environment containing F^- ions and acid, and the corrosion potential increased by about 0.17 V and 0.40 V, respectively. The increased corrosion resistance is attributed to the nano-composite structure of the TiN/ZrN layer, which has a dense columnar microstructure that is almost impermeable to corrosive media, such as H^+ and F^- ions. This TiN/ZrN layer protects the surfaces of the substrates, especially Ti, from attacks by H^+ and F^- ions in the presence of O_2. The presence of O_2 gas in the solution slightly increased the rate of anodic dissolution of the TiN/ZrN layer as compared with the solution containing H_2 gas. The corrosion rate of Ti was enhanced in the solution containing the F^- ions and O_2 gas because the F^- ions can destroy the passive Ti oxide layer and directly react with the Ti substrate to form a Ti–F^- compound. The coating of the TiN/ZrN layer greatly impeded (about 345 times) the charge transfer reaction of the anodic dissolution of Ti coupled with H^+ ion/O_2 reduction in the aqueous solution. The

improvement in the corrosion resistance of both the SS304 and Ti substrates coated with the TiN/ZrN multilayer was greater than the improvement in the sheet resistance. The TiN/ZrN coating in this study outperforms the nitride coating with single element, such as CrN and TiN coatings, in an O_2-rich environment. Therefore, this TiN/ZrN coating is a good candidate to protect the surfaces of SS304 and Ti substrates from attacks by F^- and H^+ ions in an O_2-rich URFC environment.

ACKNOWLEDGEMENTS
The authors gratefully thank the Ministry of Science and Technology of the Republic of China (Taiwan) under the contract number of MOST 103-2221-E-451-009-MY2 and NSC 101-2622-E-451-004-CC3-01 for the financial support of this research. We also thank the R&D Center of Surface Engineering in MingDao University, Taiwan, for the kindness in helping the preparation of thin films.

References

1. H.-Y. Jung, S.-Y. Huang, B.N. Popov, *J. Power Sources* 195 (2010) 1950.
2. P. Choi, *Solid State Ionics* 175 (2004) 535.
3. E.A. Cho, U.S. Jeon, H.Y. Ha, S.A. Hong, I.H. Oh, *J. Power Sources* 125 (2004) 178.
4. G. Chen, H. Zhang, H. Ma, H. Zhong, *Electrochim. Acta* 54 (2009) 5454.
5. S. Sui, L. Ma, Y. Zhai, *J. Power Sources* 196 (2011) 5416.
6. A. Hermann, T. Chaudhuri, P. Spagnol,*Int. J. Hydrogen Energy* 30 (2005) 1297.
7. J.S. Cooper, *J. Power Sources* 129 (2004) 152.
8. A. Muller, P. Kauranen, A. Vonganski, B. Hell, *J. Power Sources* 154 (2006) 467.
9. Q. Yin, A. Li, W. Wang, L. Xia, Y. Wang, *J. Power Sources* 165 (2007) 717.
10. C.-Y. Bai, M.-D. Ger, M.-S. Wu,*Int. J. Hydrogen Energy* 34 (2009) 6778.
11. H. Tawfik, Y. Hung, D. Mahajan, *J. Power Sources* 163 (2007) 755.
12. A.K. Iversen, *Corros. Sci*. 48 (2006) 1036.
13. J. Wang, J. Sun, S. Li, Z. Wen, S. Ji,*Int. J. Hydrogen Energy* 37 (2012) 1140.
14. V. Nikam, R. Reddy, *J. Power Sources* 152 (2005) 146.
15. V. Nikam, R. Reddy, *Electrochim. Acta* 51 (2006) 6338.
16. S. Wang, J. Peng, W. Lui, J. Zhang, *J. Power Sources* 162 (2006) 486.
17. J. Barranco, F. Barreras, A. Lozano, A.M. Lopez, V. Roda, J. Martin, M. Maza, G.G. Fuentes, E. Almandoz,*Int. J. Hydrogen Energy* 35 (2010) 11489.
18. K. Weil, J. Kim, G. Xia, J. Coleman, Z. Yang, *Surf. Coat. Technol.* 201 (2006) 4436.
19. D. Zhang, L. Guo, L. Duan, W.-H. Tuan,*Int. J. Hydrogen Energy* 36 (2011) 2184.
20. Y.J. Ren, C.L. Zeng, *J. Power Sources* 171 (2007) 778.
21. L. Wang, J. Sun, P. Li, J. Sun, Y. Lv, B. Jing, S. Li, S. Ji, Z. Wen,*Int. J. Hydrogen Energy* 37 (2012) 5876.
22. Y. Wang, D. Northwood,*Int. J. Hydrogen Energy* 32 (2007) 895.
23. C.J. Tavares, L. Rebout, M. Andritschky, S. Ramos, *J. Mater. Process. Technol.* 92-93 (1999) 177.
24. U.K. Wiiala, I.M. Penttinen, A.S. Korhonen, J. Aromaa, E. Ristolainen, *Surf. Coat. Technol*. 41 (1990) 191.
25. A. Rizzo, M. Signore, M. Dericcardis, L. Capodieci, D. Dimaio, T. Nocco, *Thin Solid Films* 515 (2007) 6665.
26. M. Braic, M. Balaceanu, A. Vladescu, A. Kiss, V. Braic, A. Purice, G. Dinescu, N. Scarisoreanu, F. Stokkercheregi, A. Moldovan, *Surf. Coat. Technol*. 200 (2006) 6505.
27. D. Arias, Y. Arango, A. Devia, *Appl. Surf. Sci.* 252 (2005) 1175.
28. H.-Y. Jung, S.-Y. Huang, P. Ganesan, B.N. Popov, *J. Power Sources* 194 (2009) 972.

29. H. Zhang, M. Hou, G. Lin, Z. Han, Y. Fu, S. Sun, Z. Shao, B. Yi,*Int. J. Hydrogen Energy* 36 (2011) 5695.
30. D. Zhang, L. Duan, L. Guo, Z. Wang, J. Zhao, W.-H. Tuan, K. Niihara,*Int. J. Hydrogen Energy* 36 (2011) 9155.
31. Y. Wang, D.O. Northwood, *Electrochim. Acta* 52 (2007) 6793.
32. Y. Wang, D. Northwood, *J. Power Sources* 165 (2007) 293.
33. M. Omrani, M. Habibi, R. Amrollahi, A. Khosravi,*Int. J. Hydrogen Energy* 37 (2012) 14676.
34. D.-S. Kong, Y.-Y. Feng, *J. Electrochem. Soc*. 156 (2009) C283.
35. M.-T. Lin, C.-H. Wan, W. Wu, *Thin Solid Films* 544 (2013) 162.
36. M. Kanagawa, Electron. Comm. JPN. 2 84 (2001) 36
37. I.N. Andijani, S. Ahmad, A.U. Malik, *Desalination* 129 (2000) 45.
38. A. Pozio, F. Zaza, A. Masci, R.F. Silva, *J. Power Sources* 179 (2008) 631.